

## Suppression of spurious noise sources in airfoil selfnoise measurements

Tuinstra, M; Sijtsma, P

**DOI**

[10.2514/6.2015-2689](https://doi.org/10.2514/6.2015-2689)

**Publication date**

2015

**Document Version**

Accepted author manuscript

**Published in**

Proceedings of the 21st AIAA/CEAS aeroacoustics conference

**Citation (APA)**

Tuinstra, M., & Sijtsma, P. (2015). Suppression of spurious noise sources in airfoil selfnoise measurements. In s.n. (Ed.), *Proceedings of the 21st AIAA/CEAS aeroacoustics conference* (pp. 1-16). American Institute of Aeronautics and Astronautics Inc. (AIAA). <https://doi.org/10.2514/6.2015-2689>

**Important note**

To cite this publication, please use the final published version (if applicable). Please check the document version above.

**Copyright**

Other than for strictly personal use, it is not permitted to download, forward or distribute the text or part of it, without the consent of the author(s) and/or copyright holder(s), unless the work is under an open content license such as Creative Commons.

**Takedown policy**

Please contact us and provide details if you believe this document breaches copyrights. We will remove access to the work immediately and investigate your claim.

# Suppression of spurious noise sources in airfoil self-noise measurements

Marthijn Tuinstra<sup>1</sup>

*National Aerospace Laboratory NLR, 8300 AD Emmeloord, The Netherlands*

*and*

Pieter Sijtsma<sup>2</sup>

*Pieter Sijtsma Advanced AeroAcoustics PSA3, 8091 AV Wezep, The Netherlands*

**The accurate measurement of airfoil self-noise is a challenging endeavor. Horseshoe vortices existing at the junction of a 2D airfoil section with the end plates are potent sources of spurious noise. An extension of the CLEAN-SC deconvolution algorithm is presented for the measurement of trailing edge noise and suppression of spurious noise sources. The accuracy is assessed by simulations, which show that source levels can be reconstructed within 1dB accuracy over an extensive range of frequencies. Furthermore, application on an experimental data set demonstrates the successful suppression of spurious noise and quantification trailing edge noise levels.**

## Nomenclature

$A$	=	source auto-power obtained by Conventional Beamforming
$\tilde{A}$	=	reconstructed auto-power based $\mathbf{h}$ in case of diagonal removal
$a$	=	complex pressure amplitude at source
$B$	=	source cross power
$\mathbf{C}$	=	cross-spectral matrix
$c$	=	speed of sound
$D$	=	array diameter
$f$	=	frequency
$G$	=	Green's function
$\mathbf{g}$	=	theoretical steering vector based on the Green's function
$\mathbf{H}$	=	matrix containing the diagonal elements of $\mathbf{h}\mathbf{h}^*$
$\mathbf{h}$	=	empirically determined steering vector based on source coherence
$M$	=	Mach number of uniform flow
$N$	=	number of microphones
$\mathbf{p}$	=	pressure vector
$p_N$	=	complex pressure amplitude at $N$ -th microphone
$S$	=	source auto-power based on linear least squares
$\mathbf{w}$	=	weight vector for beamforming

---

<sup>1</sup> Research Engineer, Department of Helicopters & Aeroacoustics, P.O. Box 153, email: marthijn.tuinstra@nlr.nl

<sup>2</sup> Director, Prinses Margrietlaan 13; also at Aircraft Noise & Climate Effects, Delft University of Technology, Faculty of Aerospace Engineering, The Netherlands

### Greek

- $\varphi$  = loop gain used in CLEAN algorithm  
 $\xi$  = source location

### Abbreviations

- CB = Conventional Beamforming  
CSM = Cross-spectral matrix  
KAT = Small anechoic wind tunnel  
PSF = Point Spread Function  
PWL = Sound power level  
TE = Trailing edge

## I Introduction

The accurate measurement of airfoil self-noise is often hampered by the presence of spurious noise sources. In the past cross correlation techniques<sup>1</sup> exploiting the dipole nature of trailing edge noise were used to filter out extraneous noise. More recent approaches<sup>2,3,4</sup> generally rely on acoustic array techniques.

One common source of spurious noise is encountered at the junction of the airfoil with the end-plates, resulting from the presence of a horseshoe vortex. These extraneous sources can contaminate the measured noise maps (see fig.1) and are often referred to as corner sources.

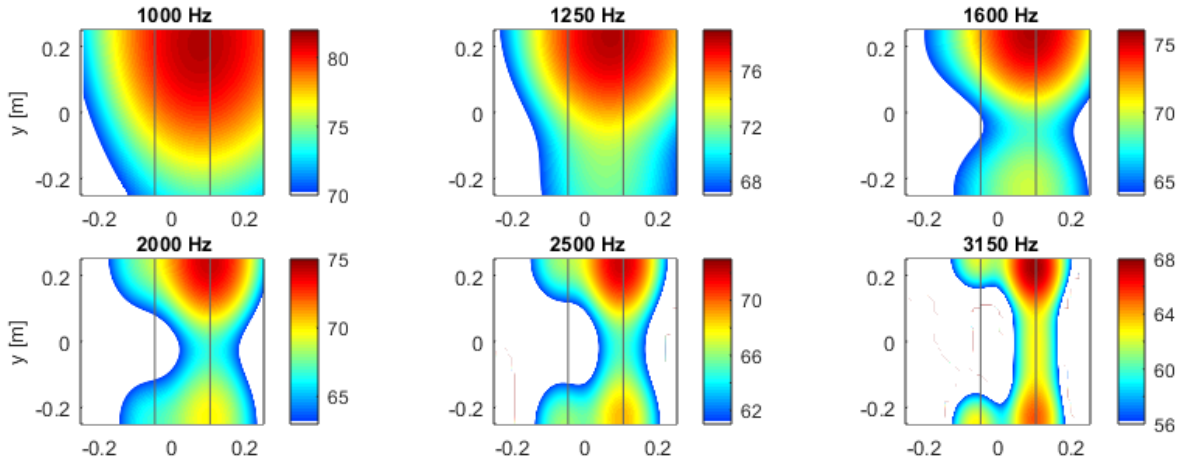


**Figure 1.** Example of source plots of airfoil trailing edge noise obtained by conventional beamforming, lines show the airfoil contours, Array diameter 0.8m, distance to trailing edge 0.64m, U=70m/s and  $\alpha=10.5^\circ$ .

Although this is a highly localized source, the array resolution is not sufficient to resolve the airfoil self-noise against the disturbance noise. When the resolution is defined as width of the main lobe at 3dB below the peak maximum (see fig.2), a rule of thumb for the resolution of an array is given by the Rayleigh criterion

$$\text{Resolution} = 1.22 \frac{cY}{Df}, \quad (1)$$

where  $f$  is the frequency,  $Y$  the distance between source and array,  $c$  the speed of sound and  $D$  is the diameter of the array.

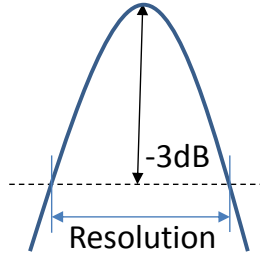


Figure 2. Array resolution.

Equation (1) applied to the case presented in fig.1 yields an array resolution of 0.34m at 1kHz. The source plot for 1kHz is therefore likely to be contaminated by corner sources entirely, which makes interpretation of trailing edge noise levels difficult.

This paper will introduce a deconvolution approach aiming at suppressing spurious noise sources in airfoil self-noise measurements. The theory behind conventional beamforming, the point spread function and a modified CLEAN-SC algorithm will be discussed in section II. This is followed by section III in which an assessment is given of the accuracy of the algorithm based on simulated source distributions. Section IV will provide a demonstration of the new algorithm applied to measurements on a DU 96-W-180 airfoil, which is followed by the conclusions.

## II Theory

### A Conventional beamforming

The notation and derivations as given by Sijtsma<sup>5</sup> will be closely followed. First, an  $N$ -dimensional vector  $\mathbf{p}$  is defined:

$$\mathbf{p} = \begin{pmatrix} p_1(f) \\ \vdots \\ p_N(f) \end{pmatrix}. \quad (2)$$

that consists of the complex frequency dependent pressure amplitudes measured at  $N$  microphone locations. Secondly, the cross-spectral matrix (CSM)  $\mathbf{C}$  is introduced by

$$\mathbf{C} = \frac{1}{2} \langle \mathbf{p} \mathbf{p}^* \rangle, \quad (3)$$

where the asterisk indicates the complex conjugate transpose. The propagation of a unit monopole source located at a position  $\vec{\xi}$ , to a microphone located at  $\vec{x}_n$  is defined by the steering vector  $\mathbf{g}$ , for example given by the Green's function of monopole in uniform flow<sup>6</sup>. The complex amplitudes  $a$  of a source located at  $\vec{\xi}$  is then obtained by minimisation of

$$J = \|\mathbf{p} - a\mathbf{g}\|^2. \quad (4)$$

The solution of this minimisation problem is

$$a = \frac{\mathbf{g}^* \mathbf{p}}{\|\mathbf{g}\|^2}. \quad (5)$$

The source auto-power is then obtained through

$$A = \frac{1}{2} |a|^2 = \frac{1}{2} a a^* = \mathbf{w}^* \mathbf{C} \mathbf{w}. \quad (6)$$

where the weight vector  $\mathbf{w}$  is given by

$$\mathbf{w} = \frac{\mathbf{g}}{\|\mathbf{g}\|^2} \quad (7)$$

Equation (6) is generally referred to as Conventional Beamforming (CB).

## B Point spread function

A theoretical derivation of the array response to a point source now follows. Suppose there is a unit source in a scan point  $\vec{\xi}_j$  that induces a CSM

$$\mathbf{C}_j = \frac{1}{2} \mathbf{g}_j \mathbf{g}_j^* \quad (8)$$

Then CB (eq. (6)) will yield source powers  $A_{jk}$  in scan points  $\vec{\xi}_k$

$$A_{jk} = \mathbf{w}_k^* \mathbf{C}_j \mathbf{w}_k \quad (9)$$

This expression is the Point Spread Function (PSF), which describes the array response of a point source. It is often found impractical to enhance array resolution by increasing the array aperture, either due to coherence loss, lack of space or source directivity. Exploitation of the PSF however, offers a powerful tool to improve array results. Both CLEAN<sup>7</sup> and the DAMAS<sup>4</sup> deconvolution algorithms are two well-known examples.

An alternative to the theoretical PSF was given by Sijtsma<sup>8</sup>, who argues that due to coherence loss, source directivity and other sources of error, the theoretical PSF does not always provide adequate means for deconvolution. An empirical PSF is therefore constructed based on the fact that main lobe and side lobes are coherent. The derivation is as follows.

The source cross-powers can be obtained from CB by

$$B_{kj} = \frac{1}{2} \langle a_k a_j^* \rangle = \frac{1}{2} \frac{\mathbf{g}_k^*}{\|\mathbf{g}_k\|^2} \langle \mathbf{p} \mathbf{p}^* \rangle \frac{\mathbf{g}_j}{\|\mathbf{g}_j\|^2} = \mathbf{w}_k^* \mathbf{C} \mathbf{w}_j \quad (10)$$

Next, the assumption is made that any coherence of scan points  $\vec{\xi}_k$  with scan point  $\vec{\xi}_j$  can be completely attributed to the PSF caused by a source located at  $\vec{\xi}_j$ . As a consequence coherent sources, sources in close proximity of each other and mirror sources will be replaced by a single source as well, which can be beneficial.

This is expressed as

$$\mathbf{w}_k^* \mathbf{C} \mathbf{w}_j = \mathbf{w}_k^* \mathbf{C}_j \mathbf{w}_j, \text{ for all } k \quad (11)$$

,which is satisfied when

$$\mathbf{C}\mathbf{w}_j = \mathbf{C}_j\mathbf{w}_j \quad (12)$$

Eq. (12) does not have a unique solution for  $\mathbf{C}_j$ . It does however, when we write

$$\mathbf{C}_j = A_j(\mathbf{h}\mathbf{h}^* - \mathbf{H}) \quad (13)$$

where  $\mathbf{H}$  is a diagonal matrix of which the diagonal elements are equal to those of  $\mathbf{h}\mathbf{h}^*$  when CB with diagonal removal (Sijtsma<sup>5</sup>, chapter 3.4) was performed and zero otherwise. Substitution of eq. (13) in eq. (12) allows to write

$$\mathbf{h} = \alpha \left( \frac{\mathbf{C}\mathbf{w}_j}{A_j} + \mathbf{H}\mathbf{w}_j \right) \quad (14)$$

in which the unknown

$$\alpha = \frac{1}{\mathbf{h}^*\mathbf{w}_j} \quad (15)$$

remains to be solved. Multiplication of eq. (14) with  $\mathbf{w}_j^*$  yields

$$\mathbf{w}_j^*\mathbf{h} = \frac{1}{\alpha} = \alpha(1 + \mathbf{w}_j^*\mathbf{H}\mathbf{w}_j) \quad (16)$$

and therefore

$$|\alpha|^2 = \frac{1}{(1 + \mathbf{w}_j^*\mathbf{H}\mathbf{w}_j)} \quad (17)$$

A solution for eq.(17) is

$$\alpha = \frac{1}{(1 + \mathbf{w}_j^*\mathbf{H}\mathbf{w}_j)^{1/2}} \quad (18)$$

Substitution of eq. (18) in eq. (14) gives

$$\mathbf{h} = \frac{1}{(1 + \mathbf{w}_j^*\mathbf{H}\mathbf{w}_j)^{1/2}} \left( \frac{\mathbf{C}\mathbf{w}_j}{A_j} + \mathbf{H}\mathbf{w}_j \right) \quad (19)$$

This is not an explicit expression when diagonal removal is applied since the right-side still contains  $\mathbf{H}$ , a diagonal matrix of which the diagonal elements consist of the auto-powers of  $\mathbf{h}$ . However, this can generally be solved via an iterative procedure taking  $\mathbf{h} = \mathbf{g}_j$  as initial value. The PSF based on spatial coherence is then defined by eq. (9) and eq.(13).

Additionally, in case of diagonal removal the source auto-powers can be reconstructed from  $\mathbf{h}$  considering

$$\tilde{A}_j = \frac{A_j}{N} \sum_{k=1}^N \frac{h_k h_k^*}{g_k g_k^*} \quad (20)$$

where  $\tilde{A}_j$  is the corrected source power.

### C CLEAN-SC algorithm applied to trailing edge noise

The original CLEAN algorithm involves the following steps:

1. Apply the CB beamforming algorithm to the scan plane,
2. search for the peak source location  $\bar{\xi}_{\max}$
3. determine the corresponding matrix  $\mathbf{C}_{\max}$ , defined by eq. (13)
4. Replace the cross-spectral matrix  $\mathbf{C}$  by  $\mathbf{C} - \varphi \mathbf{C}_{\max}$ , where the loop gain  $\varphi$  is a safety factor with  $0 < \varphi \leq 1$ .
5. Return to step 1, unless a certain stop criterion is fulfilled.

In here, the assumption is that the most likely source location is where the source map achieves a maximum. This is generally correct for incoherent and sparsely distributed sources. Application of the CLEAN-SC algorithm to the example in section I however, will result in fig.3.

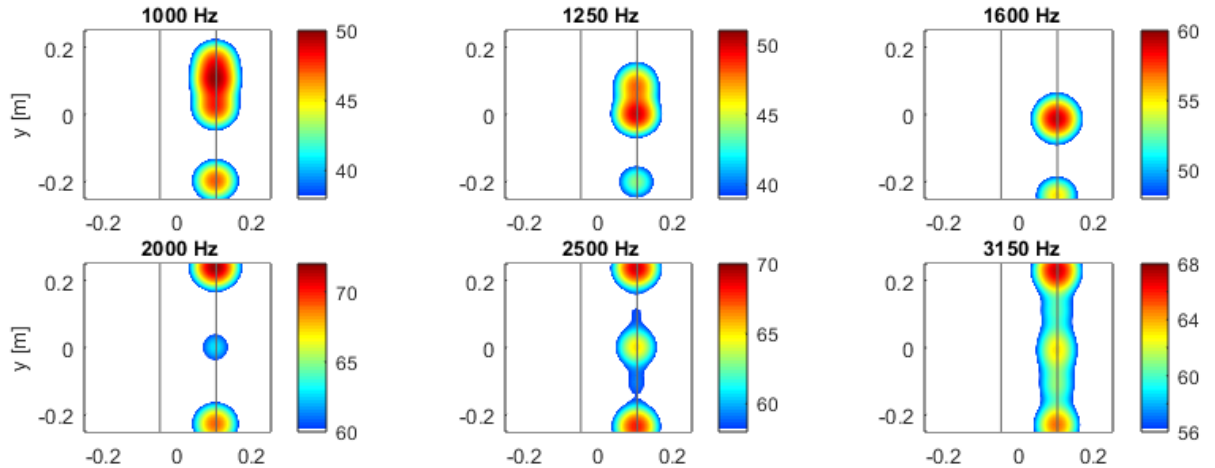


Figure 3. CLEAN maps obtained for the example given in fig.1.

Although this is a correct representation of the original source map, it is of little value for the study of trailing edge noise. In that case, the aim is to reconstruct a line source along the trailing edge, attenuating effects of spurious sources at the junction between airfoil end-plates, in order to be able to reliably express the trailing edge noise per unit span. An alternative strategy is therefore proposed. Prior to commencing the CLEAN-SC algorithm, first the contributions of trailing edge noise and spurious noise sources are removed from the CSM. This is done as follows.

First, assume  $m$  incoherent monopole sources exist at predefined locations, representing the line source at the trailing edge and other known spurious noise sources (e.g. at the junction of the airfoil with

end plates). If  $Z$  is the subset of indices of scan points at source locations and assuming there are no other sources of significance, then the cross spectral matrix induced by a point source at  $\vec{\xi}_j$ ,  $j \in Z$  is:

$$\mathbf{C}'_j = \mathbf{C} - \frac{1}{2} \sum_{k \in Z \setminus \{j\}}^{m-1} \mathbf{g}_k \mathbf{g}_k^* S_k \quad (21)$$

, where  $S_k$  is the source auto power of a source at sub-PSF resolution (below the Rayleigh limit). The steering vector  $\mathbf{h}$  is then derived from

$$\mathbf{h} = \frac{1}{(1 + \mathbf{w}_j^* \mathbf{H} \mathbf{w}_j)^{1/2}} \left( \frac{\mathbf{C}'_j \mathbf{w}_j}{A'_j} + \mathbf{H} \mathbf{w}_j \right) \quad (22)$$

, where  $A'_j$  is the auto-power derived from CB applied on  $\mathbf{C}'_j$ . The PSF based on spatial coherence for the source at  $\vec{\xi}_j$  follows from eq. (9) and

$$\mathbf{C}_j = A'_j (\mathbf{h} \mathbf{h}^* - \mathbf{H}) \quad (23)$$

The source auto-powers  $S_k$  in eq. (21) are unknown and therefore an initial estimate is needed. They cannot be obtained directly from CB since the auto-power at a single scan point contains contributions of all line source elements and spurious noise sources. From eq. (9) follows that the source auto-power at a scanpoint  $\vec{\xi}_j$  is defined as

$$A_j = \frac{1}{2} \sum_{k \in Z}^n \mathbf{w}_j^* \mathbf{g}_k \mathbf{g}_k^* \mathbf{w}_j S_k \quad (24)$$

The degrees of freedom are further restricted by demanding that line source elements should be of equal sound power. An overdetermined system of equations is defined based on eq. (24) for which the unknowns  $S_j$  are solved by means of linear least-squares regression. Since the line source elements are assumed to be of equal sound power, the number of unknowns is limited and therefore the required computational time is low. The CLEAN algorithm with sub-PSF-resolution involves the following steps:

1. Apply the CB beamforming algorithm to the scan plane.
2. Estimate source auto-powers  $S_j$  of the line source and spurious noise sources by means of linear least-squares regression
3. Select a source location  $\vec{\xi}_j$  along the trailing edge or at spurious noise source locations and determine the reduced cross spectrum matrix  $\mathbf{C}'_j$ , eq.(21).
4. Determine  $\mathbf{h}$  and the corresponding matrix  $\mathbf{C}'_j$ , defined by eq.(22) eq.(23)
5. Replace the cross-spectral matrix  $\mathbf{C}$  by  $\mathbf{C} - \varphi_j \mathbf{C}_j$  and remove scan point index  $j$  from subset  $Z$
6. Return to step 3, until all line source elements and spurious noise sources have been removed from the spectral matrix, after which the original CLEAN algorithm is applied on the remaining cross-spectral matrix.

Finally, the auto-powers of the trailing edge source elements can be reconstructed by application of eq.(20), excluding corner noise sources. This approach will be further explored based on simulations that are presented in section III.

### III Simulations

#### A Two incoherent sources in close proximity

First, the canonical case of two incoherent sources in close proximity is considered. Since the number of deconvolution steps involved is limited it allows studying the behavior of both algorithms at each individual step. Fig.4 shows the microphone layout and the source distribution that is considered. The distance between the two incoherent sources is 0.2m. A safety factor  $\varphi=0.95$  is applied in the simulations.

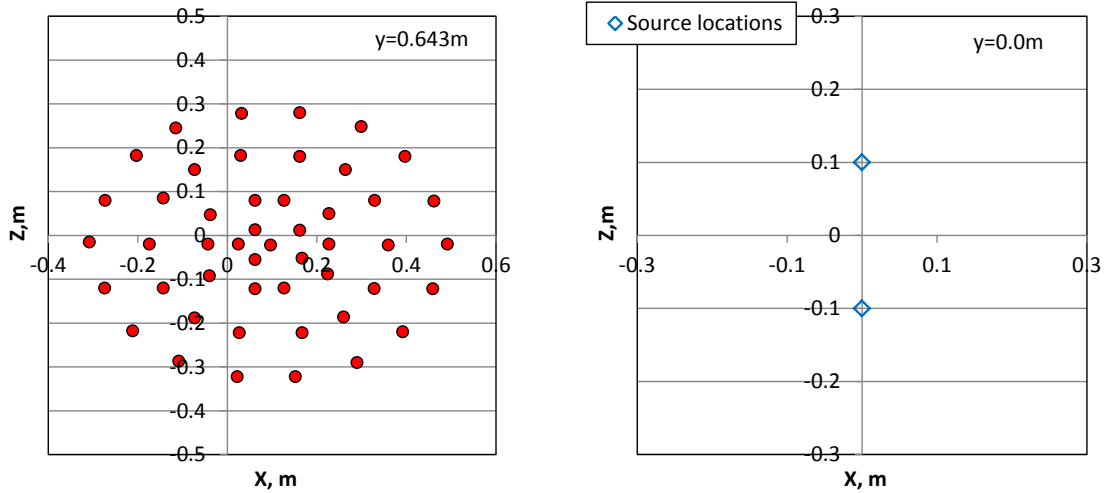
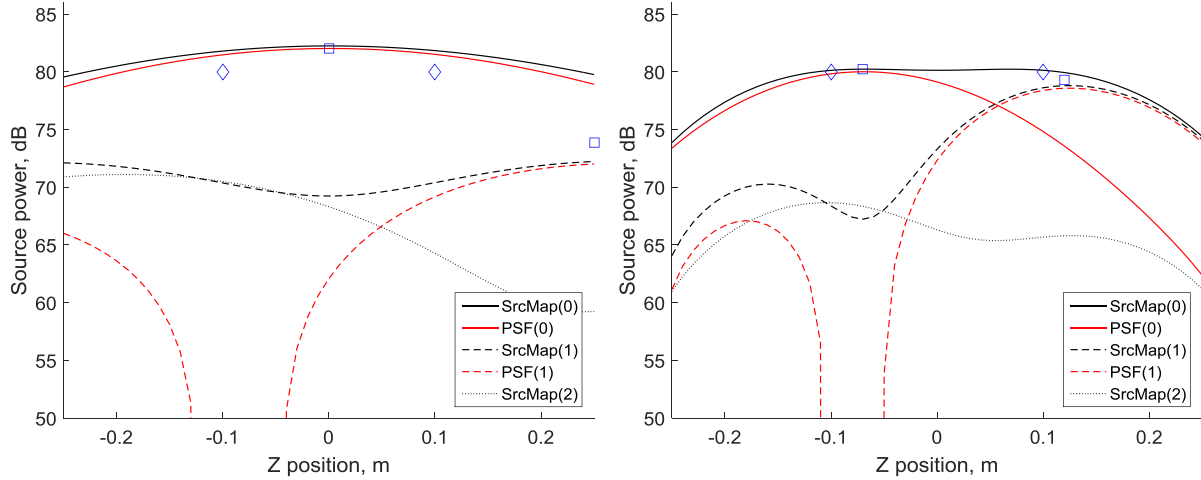
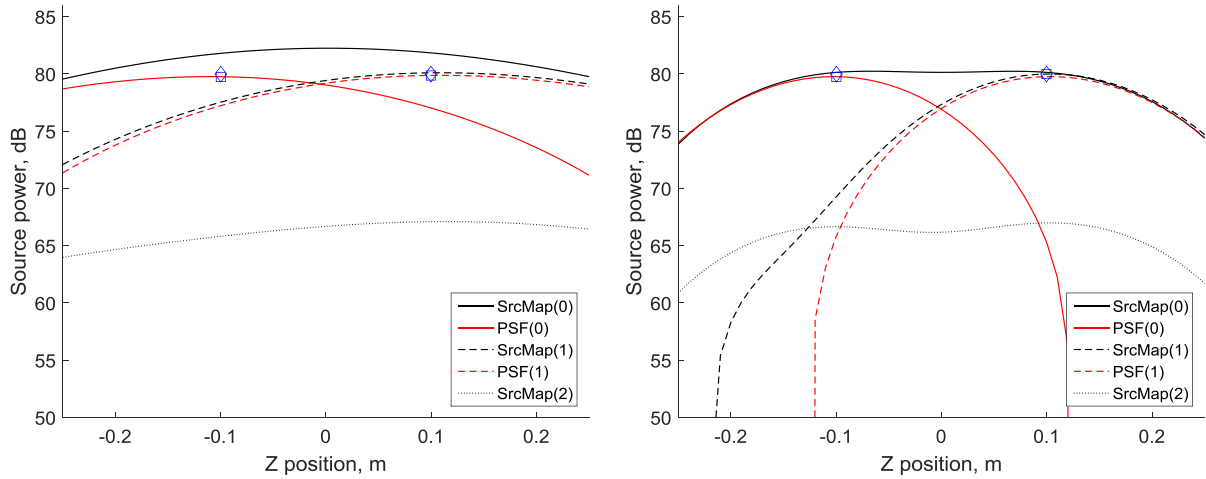


Figure 4. Left: Microphone array layout; Right: Simulated source location, sources are of unit strength and  $f=1\text{kHz}$  and  $2\text{kHz}$ .

The results at each sub-step of the ordinary CLEAN-SC algorithm are shown in fig.5. Application of CB yields a single maximum in the middle between the two sources at  $f=1\text{kHz}$  (SrcMap(0) solid black line in fig.5). At this frequency the resolution is insufficient to distinguish between the two sources. Consequently, the source location and source auto-powers, represented by the square symbols, cannot be reconstructed correctly. When the resolution is sufficient to detect two local maxima in the source map the source reconstruction improves quickly. Conventional Beamforming applied to the same case, however for  $f=2\text{kHz}$ , is shown in the right plot of fig.5. The source locations are found within 5cm and source levels are within 1dB of the actual source. A further observation is made that the empirically derived PSF in the second step (PSF(1), dashed line) corrects for the mismatch in source position in the first step, whilst conserving energy, by a side lobe at  $z \sim -0.2\text{m}$ . This particular behavior makes CLEAN-SC a robust and efficient method for deconvolution.



**Figure 5. CLEAN-SC algorithm results at each step for  $f = 1\text{kHz}$  (left) and  $f = 2\text{kHz}$  (right). Black lines indicate source maps, red line the PSF used for deconvolution, diamond symbols correspond to simulated source powers, square symbols derived source powers.**



**Figure 6. Adapted CLEAN-SC algorithm results at each step for  $f = 1\text{kHz}$  (left) and  $f = 2\text{kHz}$  (right). Black lines indicate source maps, red line the PSF used for deconvolution; diamond symbols correspond to simulated source powers, square symbols derived source powers.**

Now, we assume that the source locations are in fact known and the algorithm as described in section IIC can be applied to reconstruct the source levels. The results are shown in fig.6. Since a stronger control is exerted over deconvolution process, it is better able to decompose the cross spectral matrix in the individual source components and hence better reconstruct source levels. Source levels are found within 0.2dB of actual source levels. In fact, when the safety  $\varphi$  is set to 1 the algorithms is able to match actual source levels perfectly since there is no coherence loss incorporated in the simulations. Furthermore, inspection of the PSFs show a perfect resemblance with those based on theory, eq.(9). The overall conclusion is that when the source location is provided as input improved source power estimates are obtained by deconvolution, even at sub-PSF resolution where the ordinary CLEAN-SC algorithm fails.

## B A line source with spurious noise sources

A simulation is set up to emulate actual trailing edge noise measurement at NLR's anechoic facility KAT operating at  $M=0.2$ . A schematic of the situation is given in fig.7.

The nozzle of the KAT has  $0.38\text{m} \times 0.51\text{m}$  ( $w \times h$ ) dimensions, which positions the shear layers at  $0.19\text{m}$  from the tunnel heart. The origin of the tunnel axis system is aligned with the pitching axis of the vertically orientated airfoil. The airfoil has a  $0.15\text{m}$  chord and  $0.51\text{m}$  span and is inclined at an angle of attack of  $10.5^\circ$ . The array is positioned at  $0.64\text{m}$  from the tunnel centre line and the array centre is aligned with the trailing edge. The microphone array is identical to the microphone layout given in fig.4 and consists of 48 microphones, positioned in a manner that will result in maximum side lobe suppression over a broad range of frequencies.

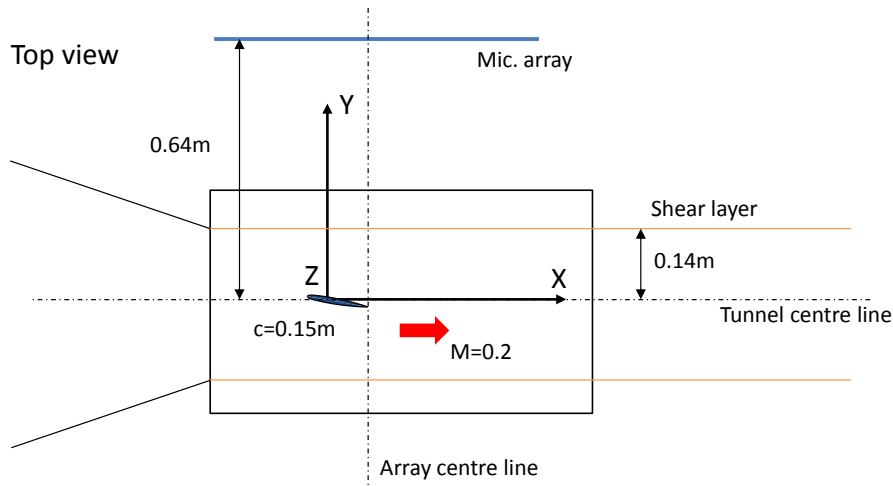


Figure 7. Top view of acoustic measurement setup on an airfoil.

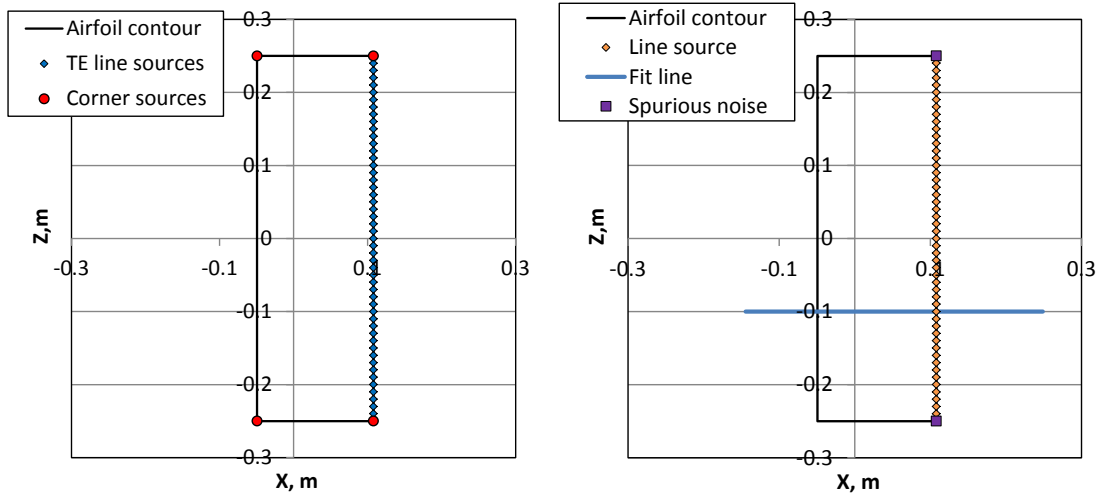


Figure 8. Left: Simulated source distribution, right: Assumed source distribution.

To simulate trailing edge noise, 49 uncorrelated monopole sources of unit strength are distributed along a line on the trailing edge at a 1cm interval, as is depicted in the left plot of fig.8. Corner source are simulated at the junctions of the airfoil with the endplate, both at the leading edge and trailing edge. From the top-left, in clockwise direction, the corner sources are given a PWL of 16, 64, 36 and 16 times that of a line source element at the trailing edge. A 0.01m resolution scan grid of 0.5m x 0.5m is used for processing that is set up so that one scan grid line overlaps with the trailing edge. This results in the source plots given in fig.9, which qualitatively agrees with the example given in fig.1.

The algorithm presented in section IIC is applied on the simulated cross power matrix. A source distribution is assumed of 49 line source elements of equal sound power and 2 spurious noise sources at the junctions. The spurious noise sources at the leading edge are purposely not considered in the reconstruction of trailing edge noise to evaluate the effect of ‘unexpected’ additional noise sources.

An overdetermined system of equation is obtained by eq. (24), considering scan points along a horizontal line at  $z = -0.1\text{m}$  (blue line in right plot of fig.8) and the scan points at the trailing edge itself. Based on linear least squares regression an initial estimate is obtained for the PWLs of the source distribution. The initial distribution obtained for  $f=1\text{kHz}$  is shown in fig.10 (left plot) by the cross symbols.

The deconvolution procedure is initiated at outside of the span  $z=\pm 0.25\text{ m}$ , moving closer towards the center span with each subsequent source that is removed from the cross spectral matrix. The rationale behind this is that any inadequacies are contained at the sources near the end plates, providing a clean source distribution at the center span, which is demonstrated by fig.10 (diamond symbols). The noise sources near the edges are contaminated by the spurious noise sources. Due to the applied safety factor in the deconvolution process and spurious noise source at the leading edge part of the energy of spurious noise source is attributed to the neighboring sources. However, over a large part of the span (88%) the correct source powers are reconstructed.

The right plot in fig.10 shows the power integrated spectrum for  $-0.2\text{m} < z < 0.2\text{m}$  (effectively 0.39m span). Over a wide range of frequencies ( $500\text{Hz} \leq f \leq 7400\text{Hz}$ ) the algorithm is able to reconstruct the source levels within 1dB accuracy. At lower frequencies ( $f < 500\text{Hz}$ ) the resolution is again insufficient to separate the trailing edge noise from spurious noise resulting in an overestimation of trailing edge noise levels. At higher frequencies ( $f > 7.4\text{kHz}$ ) the array is not able to suppress side lobes sufficiently. When the side lobes of the ‘unexpected’ sources at the leading edge overlap with the trailing edge region this causes an overestimation of noise levels, although never more than 2dB.

When comparing the power integrated spectrum based on CLEAN-SC auto-power reconstruction versus the more conventional approach of power integration it is seen that power integration consistently underpredicts source power levels by approximately 1dB. Source plots based on the filtered cross-spectral matrix, considering only sources in the region  $-0.2\text{m} < z < 0.2\text{m}$ , are shown in fig.11 and visually confirm that the corner sources are successfully suppressed.

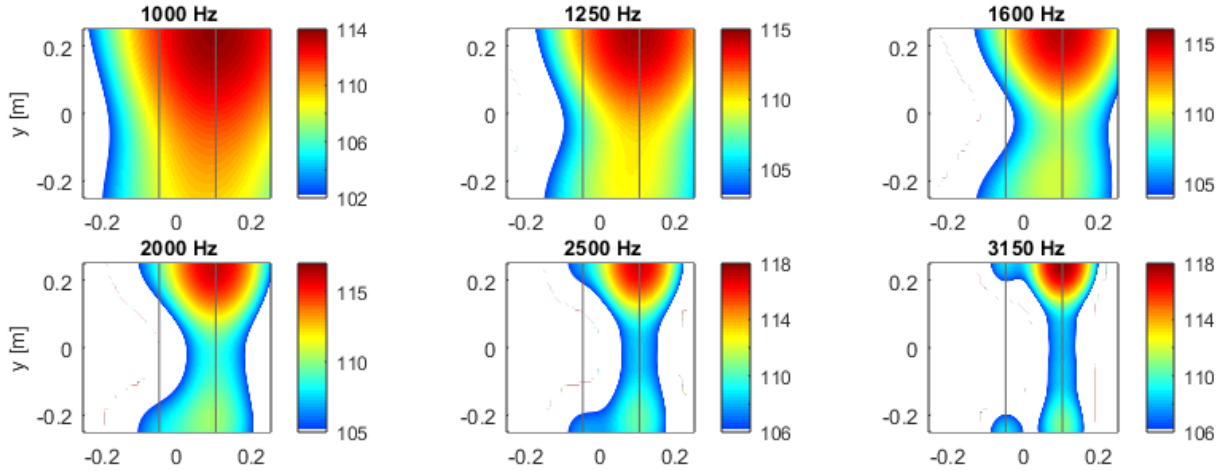


Figure 9. Simulated source plot representation of example given in fig.1.

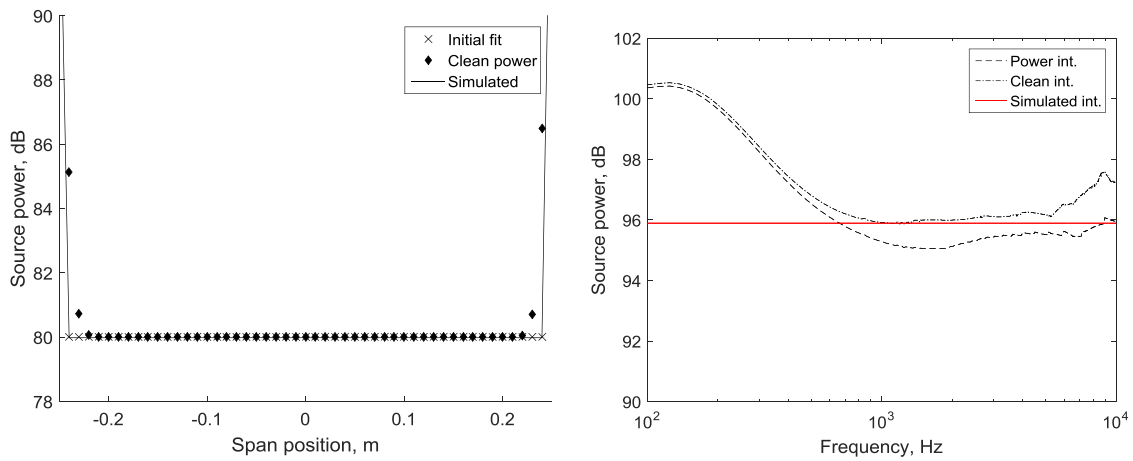


Figure 10. Source power levels, based on least squares initial estimate, CLEAN-SC and actual simulated values for  $f=1\text{kHz}$  (left) power integrated spectra (right) for  $-0.2\text{m} < z < 0.2\text{m}$ .

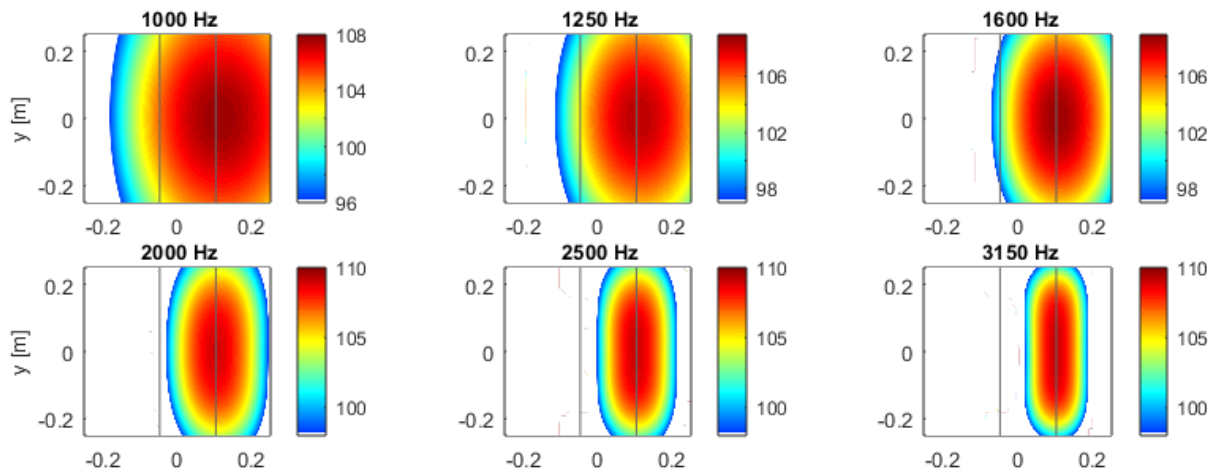
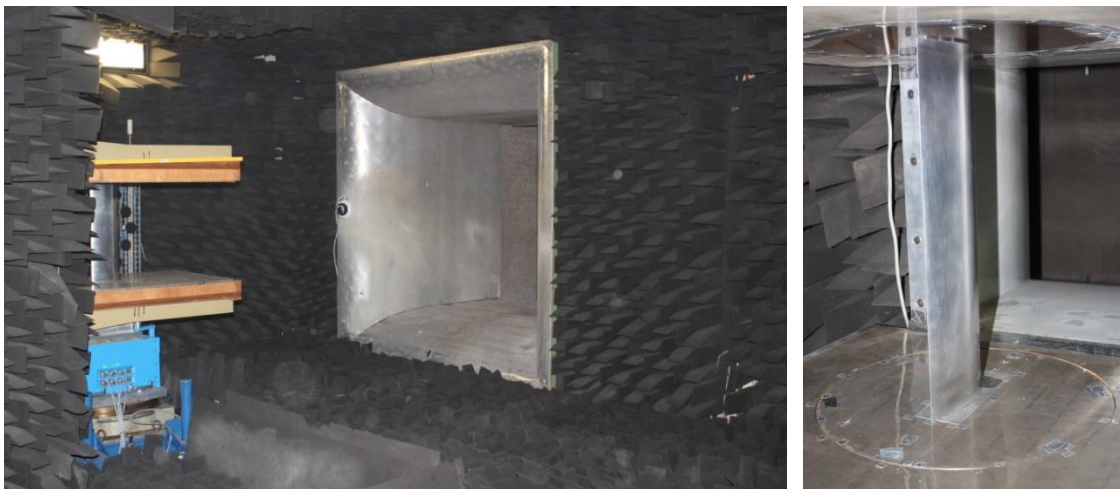


Figure 11. Simulated source plots based on the filtered cross-spectral matrix, considering only trailing edge noise sources over  $0.39\text{m}$  span .

## IV Experiments

### A Experimental setup

The tests were carried out in NLR's Small Anechoic Wind Tunnel on a DU-96-W-180 airfoil with 0.15m chord. The KAT is an open circuit, open jet wind tunnel. The test section is surrounded by a 5x5x3 m<sup>3</sup> room which is completely covered with 0.5 m foam wedges, yielding more than 99% absorption above 500 Hz. Two horizontal endplates (0.90x0.70 m<sup>2</sup>) are mounted to the upper and lower sides of the rectangular 0.38x0.51 m<sup>2</sup> nozzle, providing a semi-open test section for airfoil self-noise measurements (see fig.12). To suppress reflections, the endplates are acoustically lined with a 5.5 cm layer of sound absorbing foam covered by a 5% open perforated plate.



**Figure 12.** Pictures of the experimental setup, showing an overview of the KAT anechoic wind tunnel (left) and the profile mounted between end plates (right).

The acoustic data from the array microphones were synchronously measured using the VIPER data acquisition system. The data were acquired with a sample frequency of 51200 Hz for a measurement time of 30 s. A 500Hz high-pass filter and 25600 Hz low-pass filter were applied to the signal before the AD converter. Before the measurements, the sensitivity at 1 kHz was checked for all array microphones using a calibrated pistonphone. Frequency-dependent sensitivities of individual microphones were taken from calibration sheets. No corrections were applied for microphone directivity, because this effect is the same for the different configurations and amounts to less than 2 dB for angles up to 45° and frequencies up to 15 kHz. Phase matching of the microphones was checked prior to the measurements using a calibration source at a known position.

### B Processing

The array data are processed using the algorithm described in section IIC using an assumed source distribution corresponding to that of the simulations in section 0. This allows noise originating from the model to be separated from background and spurious noise. To improve the resolution and further suppress background noise from the tunnel, the main diagonal in the cross-power matrix (auto-powers) is

discarded. The effect of sound refraction by the tunnel shear layer is corrected using a simplified Amiet method, where the shear layer center was assumed to be at the same  $y$  location as the edge of the tunnel nozzle.

The measured pressure signals are affected by coherence loss, e.g. due to sound propagation through the shear layer. This causes measured signals at the inner part of the array to be incoherent with those at the outer rim of the array and hence an underestimation of the source levels. Therefore a spatial window is applied which reduces the effective array aperture with increasing frequency in order to reduce coherence loss effects. Furthermore, due to the non-uniform distribution of the microphones emphasis is put on the center part of the array, which is disadvantageous to the spatial resolution that can be obtained. By application of a weighting factor in the processing of the data, which is inversely proportional with the microphone density, the resolution can be improved to approach that of an array with uniform distribution of microphones<sup>5</sup>.

The array scan plane is placed in the surface plane of the airfoil. The density of the scan grid is 0.01m in both the streamwise and vertical direction, and the scan levels are normalized to a distance of 0.282 m, so that for a monopole source the peak level in the source plot corresponds to the Sound Power Level.

## **C Results**

The case of the airfoil at geometric angle of attack of  $10.5^\circ$  and a uniform flow velocity of 70m/s is considered, corresponding to the example given in the introduction section (fig.1). Fig.13 shows the CLEAN maps obtained for a span section of 0.39m. Compared to fig.3, now a more realistic distribution of sources is obtained by the deconvolution algorithm. Convincing evidence of the successful suppression of spurious noise is given by fig.14. This shows CB applied on the filtered cross spectral matrix yielding conventional source plots, however without contributions of corner sources. Qualitatively the source maps match that given in fig.11 for the simulations. The corner sources at the trailing edge are entirely suppressed. At the leading edge still some traces are found of the leading edge corner source however they are reduced in amplitude. Therefore, it is not expected to influence trailing edge noise levels.

As a final result, the integrated source power for the considered 0.39m span are presented in fig.15, both in narrow bands and 1/3 octave bands. A correction is made for background noise levels by application of the algorithm measurements for an empty wind tunnel with wind on. The correction (in  $\Delta$ dB) is derived from power integrated levels and applied on both CLEAN source integration and power integration results. When the correction is more than 3dB (signal to noise ratio equals 1) results are discarded and no longer shown.

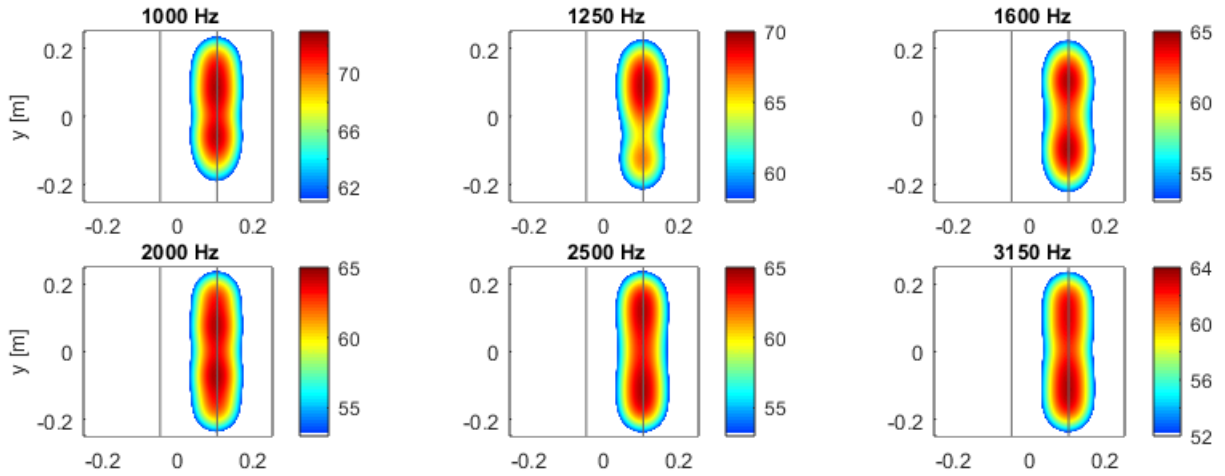


Figure 13. CLEAN maps based on the filtered cross-spectral matrix, considering only trailing edge noise sources over 0.39m span.

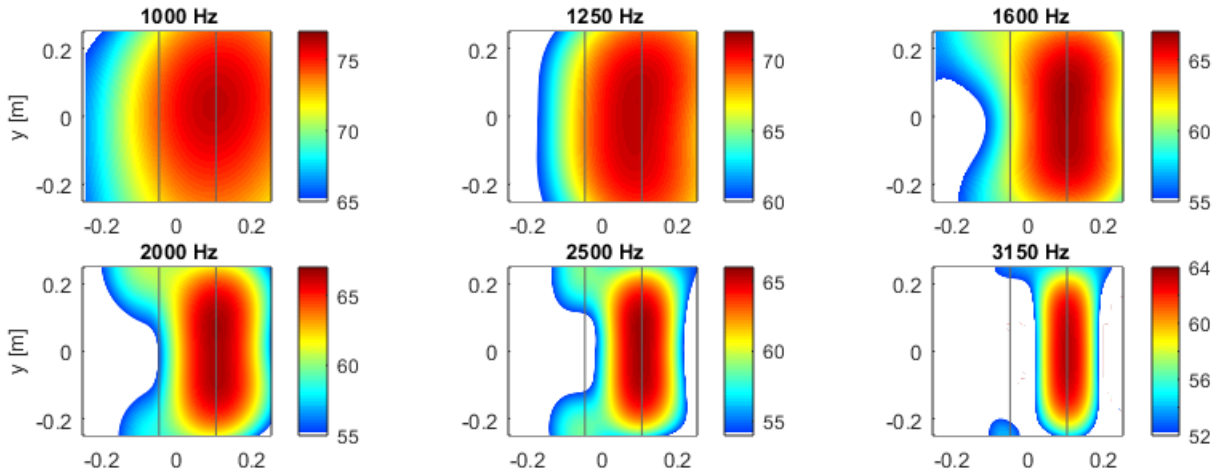


Figure 14. Source maps based on the filtered cross-spectral matrix, considering only trailing edge noise sources over 0.39m span.

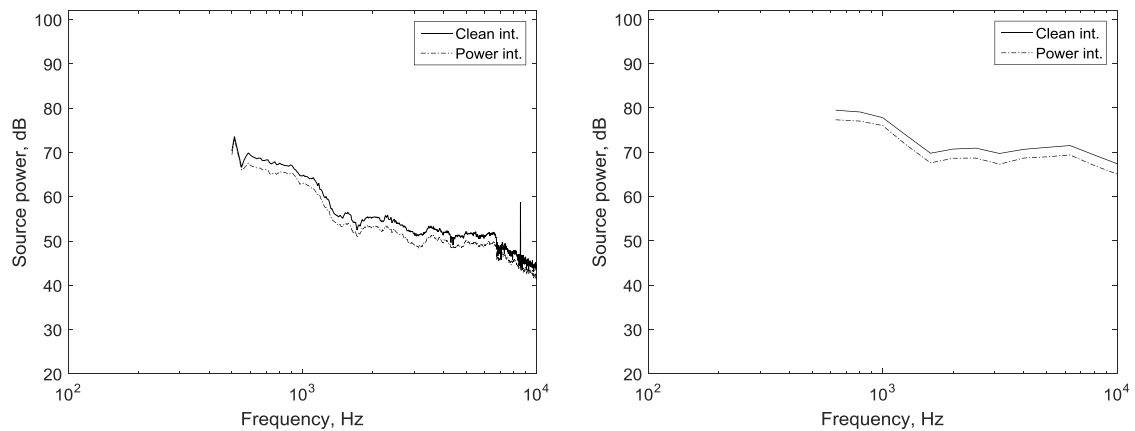


Figure 15. Power integrated spectra for  $-0.2\text{m} < z < 0.2\text{m}$  (0.39m span), corrected for background noise, represented in narrow bands ( $\Delta f=12.5\text{Hz}$ , left) and 1/3 octave bands (right).

## V Conclusions

An adapted version of the CLEAN-SC algorithm was presented for the measurement of trailing edge noise. Both in simulations and measurements spurious source were successfully suppressed, allowing the evaluation of trailing edge noise levels.

Through simulation the accuracy of the algorithm was assessed. For a frequency range of  $500\text{Hz} < f < 7400\text{Hz}$  the simulated source levels could be reconstructed within 1dB accuracy.

Although specifically developed for the measurement of trailing edge noise, the applied principles are generic. By providing knowledge of the source locations as input to the algorithm, a better estimate of source levels can be obtained, even at resolutions below the Rayleigh limit.

## References

- <sup>1</sup> T. F. Brooks, D.S. Pope and M.A. Marcolini, 'Airfoil self-noise and prediction', NASA-RP-1218, 1989.
- <sup>2</sup> S. Oerlemans, 'Wind Tunnel Aeroacoustic Tests of Six Airfoils for Use on Small Wind Turbines', NREL/SR-500-35339, May 2004.
- <sup>3</sup> F.V. Hutcheson and T.F. Brooks, 'Measurement of Trailing Edge Noise Using Directional Array and Coherent Output Power Methods', International Journal of Aeroacoustics, pp. 329-354. Vol. 1 (4), 2002.
- <sup>4</sup> T. Brooks and W. Humphreys, 'A Deconvolution Approach for the Mapping of Acoustic Sources (DAMAS) Determined from Phased Microphone Arrays', AIAA-2004-2954, 2004.
- <sup>5</sup> P. Sijtsma, 'Acoustic Beamforming for the ranking of aircraft noise', published in Aircraft Noise, VKI Lecture series 2012-02, edited by R.Denos, E. Lecomte, E.Kors and C. Schram, March 12-15, 2012.
- <sup>6</sup> A.P. Dowling and J.E. Ffowcs Williams, 'Sound and Sources of Sound', Wiley, 1983.
- <sup>7</sup> Högbom, J.A., 'Aperture Synthesis with a Non-Regular Distribution of Interferometer Baselines', Astron. Astrophys. Suppl., No. 15, 1974, pp. 417-426.
- <sup>8</sup> P.Sijtsma, 'Clean based on spatial source coherence', AIAA-2007-3436, 2007.